The Cryosphere Discuss., 8, 4281–4325, 2014
www.the-cryosphere-discuss.net/8/4281/2014/
doi:10.5194/tcd-8-4281-2014

The Cryosphere Discussions
Open Access

On the characteristics of sea ice divergence/convergence in the Southern Beaufort Sea

J. V. Lukovich, D. G. Babb, R. J. Galley, R. L. Raddatz, and D. G. Barber

Centre for Earth Observation Science (CEOS), CH Riddell Faculty of Environment, Earth, and Resources, University of Manitoba, Winnipeg, Manitoba, R3T 2N2, Canada

Received: 9 July 2014 – Accepted: 15 July 2014 – Published: 29 July 2014

Correspondence to: J. V. Lukovich (jennifer.lukovich@umanitoba.ca)

Published by Copernicus Publications on behalf of the European Geosciences Union.

Abstract

An understanding of spatial gradients in sea ice motion, or deformation, is essential to understanding of ocean-sea-ice-atmosphere interactions and realistic representations of sea ice in models used for the purposes of prediction. This is particularly true for the southern Beaufort Sea, where significant offshore hydrocarbon resource development increases the risk of oil and other contaminants dispersing into the marginal ice zone. In this study, sea ice deformation is examined through evaluation of ice beacon triplets from September to November 2009 in the southern Beaufort Sea (SBS), defined according to distance from the coastline on deployment. Results from this analysis illustrate that ice beacon triplets in the SBS demonstrate spatiotemporal differences in their evolution at the periphery and interior of the ice pack. The time rate of change in triplet area highlights two intervals of enhanced divergence and convergence in fall, 2009. Investigation of sea ice and atmospheric conditions during these intervals shows that until mid-September, all triplets respond to northerly flow, while during the second interval of enhanced divergence/convergence in October only one triplet responds to persistent northeasterly flow due to its proximity to the ice edge, in contrast to triplets located at the interior of the pack. Differences in sea ice deformation and dispersion near the pack ice edge and interior are further demonstrated in the behavior of triplets B and C in late October/early November. The results from this analysis highlight differences in dispersion and deformation characteristics based on triplet proximity to the southernmost ice edge and coastline, with implications for modeling studies pertaining to sea ice dynamics and dispersion.

1 Introduction

Sea ice motion in the Beaufort Sea is characterized by large-scale anticyclonic circulation known as the Beaufort Gyre, with reversals to cyclonic circulation during summer months and more recently throughout the annual cycle (Preller and Posey,

TCD
8, 4281–4325, 2014

1978; LeDrew et al., 1978; Proshutinsky and Johnson, 1997; Proshutinsky et al., 2002; Lukovich and Barber, 2006). Sea ice deformation, or spatial gradients in sea ice motion, in the Beaufort Sea is characterized by the formation of ridges and leads in response to atmospheric forcing and coastline geometry (Overland et al., 1995; Hutchings et al., 2011) due to compression against the multi-year ice (MYI) zone and North American continent (Hutchings et al., 2005).

Previous studies have used Lagrangian dispersion statistics and ice beacon trajectories to quantify sea ice drift and deformation in the Arctic (Colony and Thorndike, 1984, 1985; Rampal, 2008, 2009a, b). Single-particle (absolute) statistics provide a signature of large-scale circulation and capture linear time-dependence in fluctuating velocity variance characteristic of turbulent diffusion theory (Taylor, 1922; Rampal et al., 2009); departures in ice fluctuating velocity statistics from turbulent diffusion are attributed to intermittency associated with sea ice deformation and internal ice stress (Rampal et al., 2009). A two-particle (relative) statistical analysis monitors sea ice deformation, and through evaluation of buoy pair separations as a proxy of strain-rate (divergence, convergence, and strain) components combined, demonstrates heterogeneity and intermittency in the sea ice deformation field associated with space/time coupling inherent in fracturing of the sea ice cover as described by sea ice mechanics (Rampal et al., 2008; Weiss, 2013). Rampal et al. (2008) noted that a triplet or multiple-particle analysis is necessary to illustrate the deformation and small-scale kinematic features of sea ice: three-particle statistics enable a distinction between the individual strain-rate tensor components of divergence, convergence, and shear. More specifically, sea ice divergence depicts open water formation and accompanying processes such as new ice growth, brine rejection to the ocean, and heat and moisture exchange; ice convergence depicts ridge and keel formation thus contributing to ice thickness (Stern and Lindsay, 2009; Kwok and Cunningham, 2012), with implications for ice hazard detection, oil spill and contaminant transport and shipping route assessments within an increasingly industrialized Arctic.

TCD
8, 4281–4325, 2014

While sea ice deformation provides insight into both the amount of open water interspersed amongst ice, and sea ice thickness due to deformation and ridging (Kwok and Sulsky, 2010; Weiss and Marsan, 2004), statistical analysis and scaling laws for sea ice deformation provide a signature of ice mechanics and dispersion (Girard, 2009; Weiss, 2013). Recent modeling studies demonstrate the inability of current ice–ocean models to capture heterogeneity and intermittency in sea ice deformation, underscoring the need for improved understanding of ice mechanics in models (Girard et al., 2009), and resulting in the development of an alternative observational and modeling framework that incorporates anisotropic features of internal ice stress (Hutchings et al., 2011; Girard et al., 2011). Documented also in recent studies is spatial scaling dependent on season and region, with comparatively high values during summer, at the periphery of the ice pack or in first year ice (FYI) associated with loss of connectivity and coherence in the ice cover (Stern and Lindsay, 2009; Weiss, 2013). An assessment of ice beacon triplets as a measure of sea ice deformation based on distance from the continental coastline and pack ice edge, as in the present study, will contribute to an understanding of such scaling properties, and in particular dispersion near the pack ice edge periphery and interior, essential to sea ice mechanical modeling.

Previous studies have highlighted the role of forcing (wind stress) and coastline geometry in establishing lead patterns/fractures in the ice cover captured by sea ice deformation (Pritchard, 1988; Overland et al., 1995; Hutchings et al., 2005, 2011). Overland et al. (1995) demonstrated that in the Beaufort Sea for spatial scales: (i) exceeding 100 km the sea ice cover moves as an aggregate; (ii) less than 100 km the ice cover moves as an aggregate or discrete entity based on whether an elliptic (homogeneous) or hyperbolic (discrete) regime is established relative to the coastline (ice–coast interactions); and (iii) on the order of 1 km the ice cover characterized by floe (ice–ice) interactions. An assessment of the relation between stress and sea ice deformation as part of the Surface Heat Budget of the Arctic Ocean (SHEBA) campaign in the western Beaufort Sea during the 1997/98 winter demonstrated correspondence between sea ice stress measurements and regional-scale (10–100 km) deformation

TCD
8, 4281–4325, 2014

activity governed both by coastal geometry and wind direction and magnitude (Richter-Menge et al., 2002a), and highlighted the need for both stress and deformation measurements in modeling sea ice dynamics.

Overland et al. (1995) also demonstrate correspondence in atmospheric forcing and sea ice deformation in the Beaufort Sea over timescales exceeding 3 days, citing persistent winds as a contributor to a fractured ice cover due to compressional waves with comparable phase to the speed of atmospheric systems (5–10 m s^{-1}) associated with internal ice stress. An assessment of the April 1991 and 1992 Arctic Leads Experiment in the Beaufort Sea further demonstrated that for strong northerly and westerly winds lead orientation is influenced by coastal geometry and sea ice moves as a discrete entity, whereas for easterly winds the ice cover moves as an aggregate within a consolidated sea ice regime. Recent studies of observed ice conditions in the SBS note that during the 2009 *Amundsen* cruise, a storm over open water north of the Chukchi Sea generated long-period swells on 6 September 2009 that penetrated 350 km into the pack ice of the Beaufort Sea resulting in the fracture of 2–3 km floes into 50–100 m floes (Prinsenberg et al., 2010; Asplin et al., 2012). It was further shown that the swell did not extend eastward beyond 134.5° W, as determined from aerial surveys and thickness measurements on 9 September following the swell event. In the present study we examine the correspondence between changes in sea ice deformation and surface wind speed and direction relative to the (southern and westernmost) ice edge in the Beaufort Sea between September and November 2009.

Recent studies of sea ice motion in the marginal ice zone (MIZ) in the southern Beaufort Sea (SBS) analyzed ice beacon trajectories during the fall/winter of 2007/08 as part of the International Polar Year Circumpolar Flaw Lead study based on absolute, or single-particle dispersion statistics to provide a regional account of sea ice dynamics (Lukovich et al., 2011). Results from this investigation highlighted the existence of two scaling law regimes, namely in the zonal direction characteristic of westward advection and in the meridional direction characteristic of a hyperbolic (strain-dominated) regime and quasigeostrophic turbulence (Lukovich et al., 2011). Coherent ice drift features

TCD
8, 4281–4325, 2014

associated with mesoscale ice dynamics, namely loop and meander reversal events in the SBS were also investigated through analysis of relative (two-particle) Lagrangian dispersion statistics (Lukovich et al., 2014). In the present study we examine smaller-scale features and deformation characteristics of sea ice motion in the SBS based on a three-particle analysis that monitors evolution in a triangular array of ice beacons during the fall of 2009. In particular, a triplet analysis is used to provide insight into sea ice convergence and divergence that is essential to an accurate representation of sea ice dynamics in modeling studies and to our understanding of the role of sea ice dynamics in ocean-sea-ice-atmosphere interactions.

The purpose of this investigation is therefore to examine sea ice divergence and convergence in the SBS through analysis of evolution in ice beacon triplets that monitor spatiotemporal changes in sea ice motion and its gradients. Central to this investigation is an examination of sea ice conditions and atmospheric contributions to sea ice deformation and thus dispersion at varying distances from the pack ice edge in the SBS. In light of these considerations, we examine the following research questions:

1. what is the evolution in area of ice beacon triplets during the fall of 2009 and how is this evolution influenced by triplet proximity to the continental coastline and pack ice edge? (Sea ice convergence and divergence)

2. Is sea ice deformation in fall 2009 governed by ice and/or atmospheric forcing? (Sea ice and atmospheric forcing)

The results from this analysis will therefore highlight differences in dispersion characteristics as a function of distance from the ice edge based on the evolution in ice beacon triplets and smaller-scale sea ice drift features in the SBS.

TCD
8, 4281–4325, 2014

1.1 Background

Triplet analysis and (oceanic and sea ice) applications

Early studies of oceanic circulation have used multiple particles to monitor small-scale deformation and mixing as opposed to larger-scale stirring mechanisms inherent in single-particle statistical analyses. The change in the area of a triangular configuration or triplet of drifters monitors the change in flow divergence, and can be expressed as

$$\frac{1}{A}\frac{\mathrm{d}A}{\mathrm{d}t} = \frac{\partial u}{\partial x} + \frac{\partial v}{\partial y}, \tag{1}$$

where A denotes the triangle area, and u and v depict the zonal and meridional components of ocean circulation (Molinari and Kirwan, 1975; LaCasce, 2008). Negative values correspond to convergence. Additional gradients in sea ice motion or deformation characteristics such as vorticity, shearing and stretching can also be computed from changes in the triplet area through rotation of the velocity vectors (Saucier, 1955). In non-divergent flow the triplet area is conserved so that expansion in one direction is accompanied by contraction in another direction and the triangle becomes an elongated filament (Prinsenberg et al., 1998). Changes in the aspect ratio (defined as the longest leg or base divided by the height) also illustrate changes in the triplet area; increasing values indicate elongation of the triplet and filamentation or stretching of the triangular configuration, while decreasing values indicate an approach to an equilateral configuration.

Early applications of a Lagrangian triplet analysis include the investigation of (surface) drifters in the western Caribbean (Molinari and Kirwan, 1975) and in the Gulf of Mexico (LaCasce and Ohlmann, 2003). Both studies depict an increase in triplet area characteristic of non-divergent flow and displacements in response to wind forcing. It was further shown that a decrease in the aspect ratio in the Gulf of Mexico resembled a transition from non-local dispersion associated with elongation of the triangles to local mixing associated with a return to an equilateral configuration characteristic of

TCD
8, 4281–4325, 2014

turbulent dispersion (LaCasce and Ohlmann, 2003). Subsurface observations based on sulfur hexafluoride tracer release experiments in the northeast Atlantic also demonstrated filamentation of the tracer due to non-local stirring and subsequent mixing at smaller scales (Ledwell et al., 1988).

Ice beacon triplet arrays have been used in previous studies to monitor sea ice deformation off the Canadian east coast and in Antarctica (Prinsenberg et al., 1997; Heil et al., 2002, 2008, 2009, 2011). Studies of correspondence between ice stress, convergence and atmospheric forcing off the southern coast of Labrador in March 1996 showed little change in convergence within an already compact ice cover, in addition to an increase in stress with winds and decrease in stress with temperature as the icepack loses its ability to transmit pressure (Prinsenberg et al., 1997). These results are consistent with studies of derived ice motion fields using synthetic aperture radar data showing sea ice deformation and production 1.5 times higher in the seasonal than in the perennial ice zone throughout the Arctic in late fall and winter due to differences in ice strength and thickness (Kwok, 2006). Hutchings et al. (2011) through analysis of a nested beacon configuration and array with spatial scales ranging from 10 km to 140 km as part of the March 2007 Sea Ice Experiment: Dynamic Nature of the Arctic (SEDNA) campaign in the western Beaufort Sea demonstrated coherence between 140 and 20 km divergence arrays for time periods of up to 16 days in March and over shorter (sub-synoptic) timescales following May.

Studies of the evolution in triangular configurations within a 24-beacon array in the western Weddell Sea in fall, 2004 during the Ice Station POLarstern (ISPOL) experiment, indicated that changes in atmospheric circulation and winds govern sea ice deformation on weekly timescales in this region (Heil et al., 2008). More recent observational studies during the austral spring of 2007 as part of the Sea Ice Physics and Ecosystem eXperiment (SIPEX) illustrated a decrease in the influence of synoptic atmospheric forcing of sea ice drift off East Antarctic relative to earlier studies despite an anomalous increase in cyclonic intensity, and an increase in semi-diurnal motion variance. Significant divergence in the region evidenced in triplet area increases ranging

TCD
8, 4281–4325, 2014

from 230 % in the eastern to 267 % in the western portion of the region was also observed (Heil et al., 2011).

2 Methods

Sea ice drift data were determined from an array of ten ice beacons and one ice mass balance buoy launched from the CCGS *Amundsen* in the marginal ice zone of the southern Beaufort Sea in September 2009 (Fig. 1 and Table 1). From this array, five triangular configurations were selected, hereinafter referred to as triplets A to E, to monitor divergence and convergence of sea ice, with initial inter-beacon distances of approximately 11, 11, 11.5, 7, and 11 km for the shortest leg, and 15, 37, 11.5, 12.5, and 400 km for the longest leg, respectively. Triplets A to D were deployed on MYI and labeled according to their proximity to the continental coastline: triplet A was located closest to the coastline, while triplet D was located furthest from the coastline. Triplet E extended into the MIZ and was used to monitor deformation for different ice types in contrast to the other four triplets, while also demonstrating relative motion between the central pack and the marginal ice zone. Position coordinates were available for all beacons in: triplet A until 6 October; triplet B until 4 November; triplet C until 25 November; triplet D until 3 November, and triplet E until 3 October, yielding time intervals with durations of 28, 56, 77, 59, and 29 days, respectively (Table 2). Since the anticipated lifetime of the beacon batteries is at least one year, the beacon longevity may be attributed either to alternative mechanical failure or ice deformation and ridging.

Triplet areas were computed from recorded beacon latitude/longitude coordinates using Matlab® routines and Heron's formula $A = \sqrt{s(s-a)(s-b)(s-c)}$, where a, b, and c denote the length of the sides for each triplet, and $s = \frac{1}{2}(a+b+c)$. As reported in Lukovich et al. (2011), positional accuracy of the ice beacons ranged from 2.5 to 5 m based on circular and spherical error probability associated with the GPS module, while temporal accuracy was on the order of nanoseconds and thus negligible. Position accuracy for the ice mass balance buoys was

TCD
8, 4281–4325, 2014

less than 3 m according to Garmin GPS16X-HVS product Standard GPS accuracy. Error propagation analysis for the triangle area and triplet evolution according to Heron's formula yields initial error estimates on the order of $\delta_A = \frac{1}{\sqrt{8}A}\sqrt{(b^2+c^2-a^2)^2a^2+(a^2+c^2-b^2)^2b^2+(a^2+b^2-c^2)^2c^2} \sim 0.05, 0.12, 0.04, 0.04,$ 2.1 km^2 for triplets A to E, respectively. Ice and atmospheric conditions are investigated according to the spatial and temporal evolution in ice beacon triplet centroids. Ice drift velocities for each triplet centroid further highlight acceleration/deceleration in the triplet during fall, 2009.

A diagnostic known as the local meander coefficient, which is defined as the ratio of the total trajectory length to its net displacement over a given interval of time, has been used in the aforementioned studies of ice beacon triplets launched in Antarctica to monitor deviations of the beacons from their mean drift (Heil et al., 2008, 2011; Massom, 1992). Values of one indicate linear drift characteristic of the mean, whereas high values (significantly greater than one) indicate erratic drift. High meander coefficients (> 8) for the ISPOL experiment in the Weddell Sea in the austral summer of 2004 were attributed to significant anticyclonic circulation associated with tidal forcing over shallow water (< 700 m) relative to ice drift over deeper water (> 900 m) characterized by low meander coefficients (~ 4) less susceptible to tidal forcing (Heil et al., 2008). By contrast, low meander coefficient values (~ 1.1–1.8) for the SIPEX experiment off East Antarctica in the austral spring of 2007 were attributed to the dominant role of atmospheric, namely persistent wind, forcing relative to tidal forcing in this region (Heil et al., 2011). In the present study the meander coefficient is computed for the time interval during which all triplets are defined, from 9 September to 6 October 2009, since its value depends both on deployment dates and duration of the trajectories that define the beacon triplets.

Sea ice extent and type are examined using Environment Canada Canadian Ice Service (CIS) weekly ice charts, in addition to 12.5 km resolution Advanced Microwave Scanning Radiometer – EOS (AMSR-E) daily sea ice concentration data. Daily and weekly maps of sea ice concentrations illustrate spatial variability in the SBS, while

TCD
8, 4281–4325, 2014

also enabling an assessment of ice conditions in the vicinity of the triplet centroids during their evolution from September to November 2009.

Atmospheric forcing of sea ice was monitored through investigation of North American Regional Reanalysis (NARR) wind data (Mesinger et al., 2006). Atmospheric contributions to changes in sea ice deformation were investigated using daily averages of 10 m zonal and meridional winds computed from 3 hourly NARR data for the SBS to generate time series of NARR winds highlighting the existence of on-shore and off-shore winds that would contribute to changes in the sea ice deformation in fall, 2009.

3 Results and discussion

3.1 Sea ice convergence and divergence

A map of trajectories for all beacons launched in fall/winter of 2009 and 2010 illustrates the large-scale circulation pattern associated with the anticyclonic circulation in the southern segment of the Beaufort Gyre (Fig. 1). Noteworthy is the existence of small-scale variability on the order of tens of kilometers superimposed on the larger-scale westward advection, captured by meander coefficients computed for each beacon duration (Table 1). Comparatively high values (~ 1.7) are found for beacons 9, 10, and 11 launched at higher latitudes ($\sim 74.5^{\circ}$ N) relative to other beacons (~ 1.3), and included in triplets D and E, indicating more erratic ice drift at higher latitudes in the SBS in the fall of 2009. It should however be noted that these values (< 2) are smaller than those encountered in the Weddell Sea (~ 8) during the ISPOL experiment, as noted by Heil et al. (2008). Examination of ice beacon triplets also shows that they follow the same general path with increased stretching closer to the coastline until November 2009 (Fig. 1a), suggesting large-scale coherence in the pack upon which are superimposed smaller-scale features in response to forcing based on proximity to the ice edge associated with the tongue of MYI evident in the SBS at the time of deployment (Fig. 1b), as is discussed further in Sect. 3.2.

TCD
8, 4281–4325, 2014

From the array of beacons released to the west of Banks Island in September 2009, five triplets were identified according to their proximity and ice regime location (Figs. 1 and 2). Maps of triplets and their centroids highlight spatial differences in triplet evolution according to their distance from the continental coastline and southern ice edge (Fig. 2). In particular, the initial configuration of triplet A is confined to the eastern Beaufort Sea, and subsequently experiences horizontal deformation and stretching near 140° W on 9 September 2009, followed by an increase in triangular area. By contrast, triplet B, defined until 4 November 2009, initially demonstrates intervals of a zonally (horizontally) elongated configuration while advected westward until 155° W after 23 October 2009, following which the triplet area increases. Triplet C, defined until 25 November 2009, also maintains its configuration until approximately 155° W on 4 November 2009, when two beacons within the triangular configuration are interchanged. Located further north than triplet C and defined until 3 November 2009, triplet D maintains its initial configuration, with intervals when the beacons align within the meandering trajectory over spatial scales on the order of tens of kilometers in the eastern Beaufort Sea. Noteworthy are regions where the triplet D becomes "trapped" or stalled, namely near 74.5° N, 136° W, 73.5° N, 140° W, and 73.5° N, 145° W on 15 September, 7 and 15 October 2009, respectively. Triplet E, consisting of ice beacons in distinct ice regimes is distinguished by significant shearing events and deformation during the short time interval in which it is defined, namely until 3 October 2009. It should however be noted that triplet E encompasses a much larger region than other triplets, and that the southernmost beacon is located far further west than other beacons; thus triplet E is presented not for comparison with other triplets, but rather to highlight evolution in sea ice deformation within two different ice regimes.

Temporal evolution in triplet configurations is captured in the time series of triangular areas (Fig. 3), the time rate of change of which monitors ice convergence and divergence (Fig. 6). In triplet A an increase in area observed until 19 September 2009, is followed by a decline indicative of the elongated structure observed near 140° W (Fig. 2), followed by an equilibration and return to pre-existing area values until early October.

TCD
8, 4281–4325, 2014

Triplet B exhibits increased temporal variability relative to other triplets and in particular a rapid decrease in area on 15 and 21 September near 137 and 140° W (Fig. 2), and on 15 and 22 October near 147 and 150° W associated with zonal alignment of the beacons and intersection of their paths. For triplet C, a slight increase in area is followed by a decline near 17 September associated with meridional alignment of the beacons near 73° N and 137° W (Fig. 2) and a return to initial values until 3 November when the area begins to substantially increase. The increase in area in triplet B near 155° W following 24 October depicts its evolution to a more equilateral configuration (Fig. 2), whereas an increase in area for triplet C near 155° W following 3 November depicts its evolution to an elongated configuration (Fig. 2). Triplet D exhibits a decline to vanishing area values near 15–16 September as the beacons align within a trapping regime near 74.5° N and 136° W (Fig. 2), followed by a gradual increase in area that approaches the initial state until early November. For triplet E an abrupt decline in area is observed near 6 September 2009, followed by an increase that is sustained until early October. Results from the triplet area analysis show that all triplets respond to a single forcing event in September, with differences (increasing or decreasing area) providing a signature of regional small-scale constraints; in October triplet B exhibits the largest changes in area.

Temporal evolution in triangle shape is monitored through analysis of the base, height, and aspect (base-to-height) ratio for each triplet (Fig. 4). Base values decrease with increased distance from the coastline, highlighting the aforementioned enhanced stretching closest to the coastline (Fig. 4a). A gradual increase in base values is initially observed for triplets A to D until 14 September, followed by equilibration in all triplet values, with an increase near 24 October for triplet B and, further from the coastline, near 3 November for triplet C. Base values provide an interpretation of two-particle displacements or relative separation between a pair of particles: constant slopes from 19 September to 14 October indicate coherence in triplet beacon trajectories over length scales of 20, 30, and ∼ 70 km for triplets D, C, and B, respectively, while enhanced values following 24 October for triplet B and 3 November for triplet C indicate

TCD
8, 4281–4325, 2014

a change in ice drift characteristics and transition to an alternative dynamical regime. Height values capture triplet area behavior shown in Fig. 3, with vanishing values on 6 September for triplet E, from 14 to 16 September evident in triplets B, C, and D, and from 15 to 22 October for triplet B located closest to the coastline, culminating in an increase in triplet B height values following 24 October (Fig. 4a). The absence of coherence indicative of small-scale ($\sim$ 6 km) variability is evident in differences in height values for triplets A and B, which share two of the three beacons comprising the triplets.

The aspect (base-to-height) ratio further highlights differences in triplet evolution according to proximity to the ice edge and coastline (Fig. 4b). As is noted in the Introduction, decreasing values in, or negative slopes for plots of, the aspect ratios as a function of time indicate an approach to a more equilateral configuration where the triangle base and height are of comparable magnitude (aspect ratio $\sim$ 1) whereas increasing values or positive slopes indicate elongated/stretched triangles characteristic of filamentation. Triplets A, C, and to a lesser extent E, demonstrate positive slopes indicating a tendency for filamentation (short intervals of a decrease in the ratio indicate recovery from alignment near mid-September) in the early and later stages of development. By contrast, negative slopes for triplet B approaching early November depict an evolution to a more equilateral configuration shown in Fig. 2: local maxima in the aspect ratio for triplet B in September and October indicate intervals of zonal alignment and shear. A local maximum in the aspect ratio for triplet D near 15 September corresponds to beacon alignment within the trapping regime located near 74.5° N and 136° W (Figs. 2 and 3). Triplets B, C, and D thus show enhanced values characteristic of shear (increased base and reduced height) following mid-September. In October, triplet B shows enhanced aspect ratios in October, while surviving triplets C and D show sustained yet decreasing shear with increasing distance from the southern ice edge and coastline.

As previously noted, LaCasce and Ohlmann (2003) demonstrated in the study of oceanic drifter triplets an exponential increase in the triangle base and accompanying increase in height, and attributed this to the superposition of a diffusive or random-walk

TCD
8, 4281–4325, 2014

regime upon exponential stretching characteristic of shear. A similar increase in both triangle base and height in triplet B in early November in the present analysis suggest that ice deformation monitored by triplet B captures analogous behavior; namely small-scale variability associated with mixing at the pack ice edge superimposed on exponential stretching, westward advection and shear associated with anticyclonic circulation of the Beaufort Gyre, evident in the elongation of triplet C in November. As is also noted in the Introduction, LaCasce and Ohlmann (2003) and LaCasce (2008) further showed that an elongated triplet configuration provides a signature of non-local forcing due to large-scale shear (as with anticyclonic circulation of the Beaufort Gyre), whereas evolution to a more equilateral configuration provides a signature of local forcing and mixing (as at the periphery of the Beaufort Gyre in the SBS). A decrease in aspect ratios for triplet B in November in the present study thus indicates a transition to mixing, while an increase in triplet C aspect ratios in November highlights increasingly strain-dominated dispersion.

Centroid velocities for each triplet illustrate intervals of acceleration/deceleration that accompany spatiotemporal changes in triangular area, while also providing insight into spatial coherence of beacon triplets: non-local behavior is captured by similar ice drift for all beacon centroids, while local differences in ice drift are captured by differences in ice drift speed and orientation (Fig. 5). Comparison of centroid velocities highlights intervals when sea ice in the SBS is governed either by: non-local mechanisms and moves as consolidated aggregate or; local mechanisms and moves as a fractured ice cover governed by local interactions. All triplets show comparable ice velocities until late September, with a decrease in ice drift and deceleration that accompanies a reduction in triangle area near 19 15, 21, and 17 September (Figs. 3 and 5). Comparable centroid drift velocities are similarly observed for triplets B, C, and to a lesser extent D until 24 October, following which increased ice drift is observed for triplet B relative to other triplets, reflecting its sudden increase in area and evolution to a more equilateral configuration.

TCD
8, 4281–4325, 2014

Sea ice convergence and divergence are monitored through analysis of the time (daily) rate of change in triplet area (Fig. 6 and Table 3). Intervals of divergence and convergence are observed from 10 to 24 September for triplets A to E, and from 8 to 26 October for triplet B. Triplet A diverges prior to 14 September 2009 near 72.5° N, 137.5° W as evidenced in an increase in triangle area and expansion in all three vertices (Fig. 2), followed by weak convergence and divergence associated with the elongation of the triplet and decrease in triplet area on 19 September. Amplified behavior is observed for triplets B, C, and D, with increasing divergence/convergence duration with increasing distance from the coastline. Enhanced convergence (divergence) is observed for triplet B on 15 September (16), for triplet C on 16 September (17–18), and for triplet D on 14 September (17). Dissimilarity in divergence/convergence for triplets A and B despite their close proximity implies loss of coherence/fracturing in the ice cover on spatial scales on the order of ∼ 5 km in the vicinity of 72.5° N and 136.8° W. Divergent/convergent activity is observed prior to 14 September for triplet E.

During the second interval (8 to 26 October) triplet B exhibits enhanced divergence (convergence; Fig. 6) on: 8 October (11) and 15 October (20) near 145 and 147° W when beacon trajectories intersect, resulting in a near-alignment of the triplet array (Fig. 2) and vanishing area (Fig. 3). Strong divergence is observed on 21 October for triplet B associated with the filamentary structure near 151° W, prior to sustained divergence due to a significant increase in triplet area and evolution to a more equilateral configuration westward of 155° W in November (Fig. 2). By contrast, triplet C is characterized by divergence/convergence (filamentation/elongation) near 74° N, 158 and 160° W on 13 and 15 November, respectively, in a manner consistent with the observed increase in the base-to-height ratio (Figs. 2 and 4). Thus along-shear transport dominates at the periphery of the ice pack before a contiguous cover is developed in the SBS; following the development of a contiguous ice cover in late October, cross-shear transport dominates at the westernmost ice edge where ice drift is unimpeded by ice-coast interactions, in contrast to triplet C, located further from the ice edge and closer to the pack ice interior. Differences in triplets B and C in the later stages of

TCD
8, 4281–4325, 2014

evolution near 155° W in November suggest that beacons in triplet B are subject to smaller-scale forcing, whereas beacons in triplet C are subject to westward advection and shear associated with large-scale circulation of the Beaufort Gyre.

Results from this analysis demonstrate that triplets A, C, and to a lesser extent E, evolve to an elongated configuration and triplet B to a more equilateral configuration in the later stages of development. Triplet D, located furthest from the coastline, is characterized by beacon triplet alignment within trapping regimes. It is further shown that triplet area evolution furthest from (closest to) the coastline and southern ice edge is depicted by coherence in length scales of 20 km, 30 km, and ∼ 70 km for triplets D, C, and B, respectively from mid-September to October. Intervals of enhanced divergent/convergent activity are observed for all triplets in September and for triplet B in October. Differences in triplets B and C near 155° W in November depict differences in dispersion based on proximity to the coastline and ice edge in the SBS. In the next section we examine sea ice and atmospheric conditions during these intervals of enhanced divergence and convergence.

3.2 Sea ice and atmospheric forcing

Weekly CIS ice charts from 7 September 2009 to 9 November 2009 (AMSR-E sea ice data from 9 September to 14 November 2009) provide a reference of changes in ice conditions in the region encompassed by the beacon array (Fig. 7a). Noteworthy for the 7 September 2009 weekly ice chart is the tongue of multiyear ice (MYI) of 9/10 total ice concentration with floe sizes on the order of 2 to 10 km within which most ice beacons for this study were launched, surrounded by lower ice concentration regions. A reduction in sea ice extent is observed until approximately 14 September, following which an ice cover consisting of old, thick first-year and grey ice with total ice concentrations exceeding 9/10 associated with evolution in the tongue of MYI is established in the SBS. New ice begins to form along the west coast of Banks Island on 5 October. A poleward retreat in the pack ice is observed on 12 October 2009. New ice begins to form along the northern coast of the Northwest Territories near Tuktoyaktuk

TCD
8, 4281–4325, 2014

on 19 October, while ice growth connecting the marginal ice zone to the west coast of Banks Island and pack ice (Fig. 7a) indicates the onset of ice-coast interactions in this region. The 26 October ice chart shows that a band of first year ice connects the shelf to the pack ice between 135 and 150° W (depicted by ellipse in Fig. 7a) enabling the onset of ice-coast interactions with meridional motion of the pack ice. By 2 November a contiguous ice cover is formed with a band of new, thin (< 10 cm) ice at 69° N between 140 and 155° W, also evident in the 9 November ice chart, that would enable increased mobility in ice–ice/ice–coast interactions due to a weaker ice cover.

Maps of weekly AMSR-E SIC and evolution in triplet centroid positions for each week showing the proximity of each triplet to the western and southern ice edge also demonstrate that triplet A and E centroids are located closest to the southern and western (respectively) ice edge for the 14–21 September week during which both exhibit weak divergence/convergence relative to other triplets (Figs. 6 and 7b). Weak divergence/convergence relative to other triplets is also observed for triplet D from 4–12 September when it is located closest to the northwestern ice edge. By contrast, the triplet B centroid is located closest to the southernmost ice edge for the 14–21 October week when strong divergence/convergence is observed, and to both the southern- and westernmost ice edge for the 30 October–9 November week when weaker divergence is observed as the triplet evolves to a more equilateral configuration.

We examine sea ice and atmospheric contributions to sea ice deformation in the context of the two intervals during which triplets exhibit strong divergence/convergence namely from 10 to 24 September, and from 9 to 26 October (Fig. 6). In this and subsequent sections, and following the terminology for coherent oceanic and ice drift features, loop reversal events refer to the spiraling motion of a triplet beacon, in contrast to meander reversal events whereby advection exceeds rotational motion (Griffa et al., 2008; Dong et al., 2011; Lukovich et al., 2014).

During the first interval (10 to 24 September), loop reversal events are observed throughout the array, providing an indication of coherence in the ice cover (Fig. 9). Progressively smaller anticyclonic loops with increasing distance from the continental

TCD
8, 4281–4325, 2014

coast and southern ice edge and differences in the sense of the loops highlight spatial variability in the influence of small-scale constraints. More specifically, triplet A, situated at the southernmost edge of the MYI tongue within a lower (~ 70 %) ice concentration regime (Figs. 8a and 9) diverges on 11 September at the onset of a loop reversal event, and during southeasterly (on-ice) wind conditions (Fig. 10). Triplet A then converges on 20 September during a northerly (off-ice) wind regime, and is characterized by horizontal alignment at the periphery of the ice edge and Beaufort Gyre in the vicinity of 90–100 % SIC (Figs. 8a and 9). Triplet B converges (diverges) on 15 September (16) due to horizontal alignment at the southernmost ice edge following the loop reversal event (Fig. 9), and on 20 September (22) due to horizontal alignment and intersection of beacon paths within 90–100 % SIC (Figs. 8b and 9) during strong (~ 4–6 m s^{-1}) northerly (northeasterly; off-ice) wind conditions (Fig. 10). Triplet C, characterized by 90–100 % SIC (Fig. 8c) converges (diverges) on 16 September (17) due to vertical (meridional) alignment following a smaller loop reversal event experienced by one of the triplet beacons (Fig. 9) during southerly (off-ice for northernmost triplets) (northerly; on-ice) wind conditions (Fig. 10), following which the beacons travel as a coherent entity and the triplet area equilibrates until early November (Fig. 3).

At higher latitudes, and closer to the northwestern ice edge, triplet D converges (diverges) on 14 September (17) during (following) the loop reversal event experienced by all three beacons (Fig. 9), with NW to SE alignment within a 90–100 % SIC regime during northwesterly (northeasterly; on-ice) wind conditions, following which, as for triplet C, beacons evolve as a coherent entity. Triplet D located in the vicinity of 74° N and 135° W also exhibits a local rotation in this timeframe (Figs. 2 and 9) with triplet height values on the order of 100 m (Fig. 4a), in keeping with the 50–100 m peak in floe size distribution encountered to the west of 134.5° W (as a barrier to transport) due to the non-locally generated long-wave swell event documented by Prinsenberg et al. (2010) and Asplin et al. (2012). Triplet E converges on 6 September and diverges on 11 September with meridional alignment during a meander reversal event at the periphery of a lower ice concentration regime relative to the surrounding area (Figs. 8e

TCD
8, 4281–4325, 2014

and 9), capturing both small-scale variability at the edge of the ice pack in addition to shearing events and drift between the MYI and MIZ ice regimes. Results from analysis of the first interval highlight in the existence of loop reversal events in response to initial southerly and subsequent persistent northerly winds for all triplets, general coherence within the pack in September 2009, upon which is superimposed smaller-scale variability due to local ice conditions and based on proximity to the southern and northwestern MYI ice edge, before the formation of a contiguous ice cover between the pack ice and coast in late October.

During the second interval of divergent/convergent activity (8 to 26 October), triplet B, consisting of surviving beacons located closest to the southern ice edge, diverges on 9 October and exhibits a northward drift prior to convergence and collapse of beacons near 147° W within 90–100 % SIC (Figs. 8b and 9) and during northeasterly (off-ice) wind conditions (Fig. 10). Convergence of triplet B on 11 October coincides with the appearance of a lower ice concentration regime (Fig. 8b) near 145° W during southeasterly (on-ice) wind conditions, while divergence occurs within 90–100 % SIC on 15 October during northeasterly (off-ice) wind conditions (Figs. 9 and 10). Furthermore, triplet B diverges on 21 October within 90–100 % SIC at the onset of enhanced variability in sea ice concentrations (Fig. 8b), with NW to SE alignment near 150° W (Fig. 9) due to the intersection of beacon paths during strong ($\sim 6\,\mathrm{m\,s^{-1}}$) and persistent northeasterly (off-ice) wind conditions (Fig. 10).

Differences in sea ice deformation and dispersion near the pack ice edge and interior are demonstrated in the behavior of triplets B and C in late October/early November. Divergence for triplet B following 23 October reflects an increase in area (Fig. 3) depicting evolution to a more equilateral configuration near 155° W (Fig. 2) as beacons approach the westernmost edge of the ice pack uninhibited by adjacent coastlines (Fig. 7b) during northeasterly wind conditions (Fig. 10). By contrast, comparatively weak divergence for triplet C following 3 November reflects an increase in area (Fig. 3) depicting its evolution to an elongated configuration near 155° W (Fig. 2) due to its location further from the southern and westernmost ice edges (Fig. 7b) where shear effects dominate. These

TCD
8, 4281–4325, 2014

results are consistent with the aforementioned observed decrease in aspect ratios for triplet B in November (Fig. 4b) highlighting a transition to mixing near the western ice edge (uninhibited by ice-coast interactions following the development of a contiguous ice cover in late October) in response to northeasterly winds; in addition to an increase in triplet C aspect ratios in November highlighting increasingly strain-dominated dispersion further from the ice edge and closer to the pack interior. Differences in sea ice divergence and convergence for triplets B and C in the later stages of evolution near 155° W (Fig. 6) also indicate that beacons located closest to the (western) ice edge in triplet B are subject to smaller-scale forcing and cross-shear transport, whereas beacons located further from the ice edge are subject to westward advection and shear associated with large-scale circulation of the Beaufort Gyre.

Enhanced variability near the ice edge is also evident in the early stages of evolution in triplets D and A, located closest to the northwestern and southwestern ice edge, respectively, of the MYI ice tongue in early September. More specifically, triplet D beacons initially travel perpendicular to the ice edge until the onset of strong northerly winds in mid-September, captured in constant base, height, and aspect ratio values until 12 September (Figs. 7b, 3 and 4). Triplet A exhibits an increase in the base and height values, with a more rapid increase in the former, indicating the aforementioned superposition of stretching and diffusive behavior characteristic of cross-shear transport witnessed in the late stages of evolution for triplet B. A more gradual increase in the aspect ratio values (Fig. 4) relative to other beacons further suggests a transition from cross-shear to along-shear transport for triplet A with increasing distance from the southwestern ice edge.

Results from this analysis suggest that intervals of enhanced divergence/convergence for all triplets early in the season (September) provide a signature of loop reversal events and small-scale variability in response to persistent northerly winds, while intervals of enhanced divergence/convergence for triplet B later in the season provide a signature of significant dynamic variability and intersection of the beacon paths in response to persistent northeasterly winds due to a fractured and

TCD
8, 4281–4325, 2014

highly mobile ice cover near the southern and westernmost ice edge. Spatial variability in triplets D and E located near the northernmost ice edge in early- to mid-September (Figs. 7b and 8d, e) captured by comparatively high meander coefficients (Table 1), coherence over shorter length scales at higher latitudes from mid-September to mid-October (Fig. 4a), in addition to variability in divergence/convergence of triplet B located near the southern (western) ice edge until late October (early November) (Figs. 7b and 8b) further highlights differences in dispersion characteristics between the periphery and interior of the ice pack.

Overland et al. (1995) demonstrated that over length scales ranging from ice floe interactions at 1 km to 100 km a hyperbolic (discontinuous) ice regime is established in response to northerly and westerly winds due to ice-coast interactions, whereas an elliptic (diffusive) regime is established in response to easterly winds and when the pack ice is not contiguous with the coast. In the present analysis, triplets B, C, and D all show enhanced aspect ratios and intervals of divergence/convergence characteristic of shear in response to northerly winds following mid-September, as they travel parallel to the southern (B and C) and northwestern (D) ice edge defined by the tongue of MYI, in a manner consistent with the hyperbolic regime described by Overland et al. (1995). Similarly in October, triplet B shows enhanced shear, and triplets C and D decreasing shear with increasing distance from the southern ice edge during predominantly northeasterly wind conditions and prior to the development of a contiguous ice cover between the pack ice and coast. However, triplet B evolves to a more equilateral configuration characteristic of cross-shear transport and mixing at the western ice edge in November in response to northeasterly winds, whereas triplet C, located further from the ice edge, continues to experience along-shear transport. Similarly, beacons comprising triplets A and D located near the northwestern and southwestern edge of the MYI tongue travel perpendicular to the ice edge in the early stages of evolution, highlighting differences in dispersion at the pack ice edge and interior.

Richter-Menge et al. (2002a) also documented contributions from coastal geometry and wind direction to deformation activity in the southern Beaufort Sea, noting

TCD
8, 4281–4325, 2014

propagation of leads away from the shore with consolidation of the seasonal and perennial ice zone, and found coherence in sea ice drift and deformation over spatial scales of 200 km. Furthermore, Stern and Lindsay (2009) found reduced deformation within the MYI regime – as was found in the present study for triplets C and D during intermediate stages of evolution within the pack interior – in addition to "localization" describing the strengthening of deformation at the smallest scales in support of a fracture as opposed to continuum description of ice deformation. Results from the present analysis confirm these findings and further illustrate through evaluation of beacon triplets and small-scale deformation, spatial variability in dispersion at the pack ice edge and interior, with enhanced cross-shear transport in response to off-ice wind conditions. In addition, weak divergence/convergence implies an approach to a more equilateral configuration; strong divergent/convergent activity suggests strong shear associated with along-shear transport.

These results are also consistent with those found in Lukovich et al. (2011), whereby zonal dispersion is characterized by the ballistic regime associated with anticyclonic circulation and westward advection at the southern segment of the Beaufort Gyre; and the hyperbolic (strain-dominated) regime associated with northward and southward displacements in the meridional direction. In the present study, differences in the latter stages of evolution in triplets B and C document similar behavior in terms of westward advection further from the ice edge and increased diffusive behavior associated with cross-shear transport at the western pack ice edge not contiguous with the coast.

It is also interesting to note that ice beacon trajectories track the memory of the ice edge and act as a prelude to the fracturing of the ice cover and polynya openings (Fig. 9), in a manner consistent with the observation that directionality and history govern regional ice dynamics (Coon et al., 1992; Overland et al., 1995). Beacon trajectories associated with triplets B and D in October and November follow both the southern and northern ice edges at the periphery of the MYI tongue in the SBS established/evident in mid-September (Fig. 9, left upper panel). Furthermore, loop reversal events associated with increased divergent/convergent activity in triplets B and C in

TCD
8, 4281–4325, 2014

mid-September provide a signature of lower ice concentration regimes that emerge in mid-October (Fig. 9). Correspondence between beacon trajectories, triplet evolution and upcoming and antecedent ice conditions at the pack ice edge highlight the nature of spatiotemporal coupling in sea ice drift and dispersion in fall, with implications for forecasting and prediction.

4 Conclusions

In this study we investigate sea ice divergence and convergence in the southern Beaufort Sea from September to November 2009, based on an assessment of ice beacon triplets defined according to their distance from the coastline and southern ice edge, with triplet A (E) centroids located closest to (furthest from) the continental coastline. Results from this analysis highlight differences in dispersion at the periphery and interior of the ice pack. Investigation of sea ice divergence and convergence shows enhanced stretching closer to the coastline, evident in decreasing triplet base values with increasing distance from the coastline. Triplets defined according to their proximity to the coastline and southern ice edge also exhibit spatiotemporal differences in their evolution: triplets A, C, and E evolve to an elongated configuration characteristic of a filament, whereas triplet B evolves to a more equilateral configuration westward of 155° W following 23 October 2009. Triplet D is confined to the eastern segment of the Beaufort Sea until November 2009. It is further shown that triplet area evolution furthest from (closest to) the coastline and southern ice edge is depicted by coherence in length scales of 20 km, 30 km, and ~ 70 km for triplets D, C, and B, respectively from mid-September to October.

The time rate of change in triplet area highlights two intervals of enhanced divergence and convergence in fall, 2009: one interval in September (from 10 to 24 September) for triplets A to E, and a second interval in October (from 9 to 26 October) for triplet B. Investigation of sea ice and atmospheric conditions during these intervals of enhanced divergence/convergence show that until mid-September, all triplets respond

TCD
8, 4281–4325, 2014

to northerly flow. Loop reversal events observed throughout the array provide an indication of coherence in the ice cover; progressively smaller anticyclonic loops at higher latitudes and differences in the sense of the loops highlight spatial variability associated with local ice conditions and proximity to the southern and western MYI ice edge, prior to the formation of a contiguous ice cover between the pack ice and coast in late October. During the second interval of divergent/convergent activity (9 to 26 October) enhanced divergence/convergence is observed for triplet B at the southern ice edge. Differences in triplets B and C near 155° W in November illustrate differences in dispersion at the periphery and interior of the ice pack based on proximity to the western ice edge in the SBS: triplet B evolves to a more equilateral configuration captured in decreasing aspect ratios indicative of mixing near the westernmost ice edge in response to northeasterly winds, unimpeded by adjacent coastlines, whereas triplet C evolves to an elongated configuration captured by increasing aspect ratio values indicative of strain-dominated dispersion further from the ice edge and closer to the pack interior.

Results from this investigation are in keeping with earlier studies documenting hyperbolic (discontinuous) and elliptic (diffusive) ice regimes in the SBS in response to northerly and westerly, and easterly and free drift conditions, respectively, while further highlighting spatial variability in dispersion characteristics within the ice pack based on proximity to the coastline and ice edge. Following mid-September, triplets B, C, and D show enhanced aspect ratios and intervals of divergence/convergence representative of shear in response to northerly winds as they travel parallel to southern (B and C) and northwestern (D) MYI edge in a manner consistent with the hyperbolic regime. Similarly, in October, triplet B exhibits enhanced shear closest to the ice edge, and triplets C and D reduced shear in response to predominantly northeasterly winds, prior to the development of a contiguous ice cover between the ice pack and continental coast. However, in late October/early November, triplet B experiences cross-shear transport and mixing characteristic of an elliptic regime in response to northeasterly winds at the western edge of the ice pack, in contrast to triplet C, which continues, further from the ice edge, to experience along-shear transport characteristic of the hyperbolic regime.

TCD
8, 4281–4325, 2014

The use of ice beacon triplets presents an approach that complements spatial scaling analyses through an assessment of sea ice deformation at the pack ice edge and interior. In demonstrating a strong sea ice deformation response to persistent northerly winds throughout the ice pack in September 2009, and to persistent northeasterly winds at the periphery of the ice pack in November 2009, the results from this analysis underline the importance of atmospheric forcing and proximity to the coastline and ice edge as the pack ice becomes contiguous with the continental coastline during fall. Correspondence between beacon trajectories, triplet evolution and upcoming and antecedent ice conditions at the pack ice edge further highlight the nature of spatiotemporal coupling in sea ice drift and dispersion in fall, with implications for forecasting and prediction. An understanding of differences in dispersion and deformation at the ice edge and interior will be of increasing importance with continued loss in MYI, decline in summertime sea ice extent, sea ice edge retreat and, as is illustrated in the present ice beacon triplets analysis, the establishment of a sea ice regime characteristic of the marginal ice zone and increased mixing at the pack ice edge. Of interest for future modeling work and field campaigns is an assessment of sea ice deformation impacts on ocean-sea-ice-atmosphere dynamic interactions and turbulent exchange between the ocean and the atmosphere under varying ice and atmospheric conditions, which would contribute to improved representation of sea ice dispersion in modeling studies used for the purposes of prediction.

Acknowledgements. Funding for this study was provided by the Canadian Networks of Centres of Excellence (NCE) program and Canada Research Chairs (CRC) grant (D. G. Barber); and Aboriginal Affairs and Northern Development Canada award (D. Babb). This is a contribution to ArcticNet and the Arctic Science Partnership (ASP). We dedicate this paper to our colleague, K. Hochheim, who lost his life while conducting sea ice research in the Canadian Arctic.

TCD
8, 4281–4325, 2014

References

Asplin, M. G., Galley, R., Barber, D. G., and Prinsenberg, S.: Fracture of summer perennial sea ice by ocean swell as a result of Arctic storms, J. Geophys. Res., 117, C06025, doi:10.1029/2011JC007221, 2012.

Barber, D. G., Galley, R., Asplin, M. G., De Abreu, R., Warner, K.-A., Pućko, M., Gupta, M., Prinsenberg, S., and Julien, S.: Perennial pack ice in the southern Beaufort Sea was not as it appeared in the summer of 2009, Geophys. Res. Lett., 36, L24501, doi:10.1029/2009GL041434, 2009.

Dong, C., Liu, Y., Lumpkin, R., Lankhorst, M., Chen, D., McWilliams, J. C., and Guan, Y.: A scheme to identify loops from trajectories of oceanic surface drifters: an application in the Kuroshio extension region, J. Atmos. Ocean. Tech., 28, 1167–1176, doi:10.1175/JTECH-D-10-05028.1, 2011.

Girard, L., Weiss, J., Molines, J. M., Barnier, B., and Bouillon, S.: Evaluation of high-resolution sea ice models on the basis of statistical and scaling properties of Arctic sea ice drift and deformation, J. Geophys. Res.-Oceans, 114, C08015, doi:10.1029/2008JC005182, 2009.

Girard, L., Bouillon, S., Weiss, J., Amitrano, D., Fichefet, T., and Legat, V.: A new modeling framework for sea-ice mechanics based on elasto-brittle rheology, Ann. Glaciol., 52, 123–132, 2011.

Guest, P. S. and Davidson, K. L.: Meteorological triggers for deep convection in the Greenland Sea, deep convection and deep water formation in the oceans, in: Proceedings of the International Monterey Colloquium on Deep Convection and Deep Water Formation in the Oceans, edited by: Chu, P. C. and Gascard, J. C., Elsevier Oceanography Series, 57, 369–375, 1991.

Guest, P. S., Davidson, K. L., Overland, J. E., and Frederickson, P. A.: Atmosphere-Ocean Interaction in the Marginal Ice Zones of the Nordic Seas, Arctic Oceanography: Marginal Ice Zones and Continental Shelves, Coast. Estuar. Stud., 49, 51–95, 1995.

Heil, P. and Hibler, W. D.: Modeling the high-frequency component of Arctic sea ice drift and deformation, J. Phys. Oceanogr., 32, 3039–3057, 2002.

Heil, P., Hutchings, J. K., Worby, A. P., Johansson, M., Launiainen, J., Haas, C., and Hibler, W. D.: Tidal forcing on sea-ice drift and deformation in the western Weddell Sea in early austral summer, 2004, Deep-Sea Res. Pt. II, 55, 943–962, 2008.

TCD
8, 4281–4325, 2014

Heil, P., Massom, R. A., Allison,I, Worby, A. P., and Lytle, V. I.: Role of off-shelf to on-shelf transitions for East Antarctic sea ice dynamics during spring 2003, J. Geophys. Res.-Oceans, 114, C09010, doi:10.1029/2008JC004873, 2009.
Heil, P., Massom, R. A., Allison, I., and Worby, A. P.: Physical attributes of sea-ice kinematics during spring 2007 off East Antarctica, Deep-Sea Res. Pt. II, 58, 1158–1171, 2011.
Hibler, W. D.: Dynamic thermodynamic sea ice model, J. Phys. Oceanography, 9, 815–846, 1979.
Hutchings, J. K. (Ed.): The Sea Ice Experiment: Dynamic Nature of the Arctic (SEDNA), Applied Physics Laboratory Ice Station, APLIS 2007 Field Report IARCTP09-0001, International Arctic Research Centre, University of Alaska, Fairbanks, AK, 2009.
Hutchings, J. K. and Hibler III, W. D.: Small-scale sea ice deformation in the Beaufort Sea seasonal ice zone, J. Geophys. Res., 113, C08032, doi:10.1029/2006JC003971, 2008.
Hutchings, J. K., Heil, P., and Hibler III, W. D.: Modeling linear kinematic features in sea ice, Mon. Weather Rev., 133, 3481–3497, 2005.
Hutchings, J. K., Roberts, A., Geiger, C., and Richter-Menge, J.: Spatial and temporal characterization of sea-ice deformation, Ann. Glaciol., 52, 360–368, 2011.
Kwok, R.: Contrasts in sea ice deformation and production in the Arctic perennial and seasonal ice zones, J. Geophys. Res., 111, C11S22, doi:10.1029/2005JC003246, 2006.
Kwok, R. and Cunningham, G. F.: Deformation of the Arctic Ocean ice cover after the 2007 record minimum in summer ice extent, Cold Reg. Sci. Technol., 76–77, 17–23, 2012.
Kwok, R. and Sulsky, D.: Arctic Ocean sea ice thickness and kinematics: satellite retrievals and modeling, Oceanography, 23, 134–143, 2010.
LaCasce, J. H.: Lagrangian statistics from oceanic and atmospheric observations, Lect. Notes Phys., 744, 165–218, 2008.
LeDrew, E. F., Johnson, D., and Maslanik, J. A.: An examination of atmospheric mechanisms that may be responsible for the annual reversal of the Beaufort Sea ice field, Int. J. Climatol., 11, 841–859, 1991.
Lukovich, J. V. and Barber, D. G.: Atmospheric controls on sea ice motion in the southern Beaufort Sea, J. Geophys. Res., 111, D18103, doi:10.1029/2005JD006408, 2006.
Lukovich, J. V., Babb, D. G., and Barber, D. G.: On the scaling laws derived from ice beacon trajectories in the southern Beaufort Sea during the International Polar Year – circumpolar flaw lead study, 2007–2008, J. Geophys. Res., 116, C00G07, doi:10.1029/2011JC007049, 2011.

TCD
8, 4281–4325, 2014

Massom, R. A.: Observing the advection of sea ice in the Weddell Sea using buoy and satellite passive microwave data, J. Geophys. Res., 97, 15559–15572, 1992.
Mesinger, F., DiMego, G., Kalnay, E., Mitchell, K., Shafran, P. C., Ebisuzaki, W., Jovic, D., Woollen, J., Rogers, E., Berbery, E. H., Ek, M. B., Fan, Y., Grumbine, R., Higgins, W., Li, H., Lin, Y., Manikin, G., Parrish, D., and Shi, W.: North American regional reanalysis, B. Am. Meteorol. Soc., 87, 343–360, 2006.
Molinari, R. and Kirwan, A. D.: Calculations of differential kinematic properties from Lagrangian observations in western Caribbean Sea, J. Phys. Oceanogr., 5, 483–491, 1975.
Overland, J. E.: Potential Arctic change through climate amplification processes, Oceanography, 24, 176–185, 2011.
Preller, R. B. and Posey, P. G.: A numerical model simulation of a summer reversal of the Beaufort Gyre, Geophys. Res. Lett., 16, 69–72, 1989.
Prinsenberg, S. J., van der Baaren, A., Fowler, G. A., and Peterson, I. K.: Pack ice stress and convergence measurements by satellite-tracked ice beacons, Oceans 97 MTS/IEEE Conference, Halifax, Canada, Oceans '97 MTS/IEEE Conference Proceedings, 6–9 October, Vols. 1 and 2, 1283–1289, 1997.
Prinsenberg, S., Peterson, I., Barber, D., and Asplin, M.: Long period swells break up the Canadian Beaufort Sea pack ice in September 2009, Twentieth (2010) International Offshore and Polar Engineering Conference, Beijing, China, 20–26 June 2010, 20–25, 1998.
Prinsenberg, S. J., Fowler, G. A., and van der Baaren, A.: Pack ice convergence measurements by GPS-ARGOS ice beacons, Cold Reg. Sci. Technol., 28, 59–72, doi:10.1016/S0165-232X(98)00013-5, 2010.
Pritchard, R. S.: Mathematical characteristics of sea ice dynamics models, J. Geophys. Res., 93, 15609–15618, 1988.
Proshutinsky, A. and Johnson, M. A.: Two circulation regimes of the wind driven Arctic Ocean, J. Geophys. Res., 102, 12493–12514, 1997.
Proshutinsky, A., Bourke, R. H., and McLaughlin, F. A.: The role of the Beaufort Gyre in Arctic climate variability: seasonal to decadal climate scales, Geophys. Res. Lett., 29, 2100, doi:10.1029/2002GL015847, 2002.
Rampal, P., Weiss, J., Marsan, D., Lindsay, R., and Stern, H.: Scaling properties of sea ice deformation from buoy dispersion analysis, J. Geophys. Res., 113, C03002, doi:10.1029/2007JC004143, 2008.

TCD
8, 4281–4325, 2014

Rampal. P., Weiss, J., Marsan, D., and Bourgoin, M.: Arctic sea ice velocity field: general circulation and turbulent-like fluctuations, 114, C10014, doi:10.1029/2008JC005227, 2009a.
Rampal, P., Weiss, J., and Marsan, D.: Positive trend in the mean speed and deformation rate of Arctic sea ice, 1979–2007, J. Geophys. Res., 114, C05013, doi:10.1029/2008JC005066, 2009b.
Richter-Menge, J. A., McNutt, S. L., Overland, J. E., and Kwok, R.: Relating Arctic pack ice stress and deformation under winter conditions, J. Geophys. Res., 107, 8040, doi:10.1029/2000JC000477, 2002a.
Richter-Menge, J. A., Elder, B., Claffey, K., Overland, J., and Salo, S.:, In situ sea ice stresses in the western Arctic during the winter of 2001–2002, in: Proceedings of the 16th IAHR International Symposium on Ice, 2–6 December, edited by: Squire, V. A. and Langhorne, P. J., Univ. of Otago, Dunedin, New Zealand, 131–138, 2002b.
Saucier, W. J.: Principles of Meteorological Analysis, University of Chicago Press, Chicago, IL, 438 pp., 1955.
Taylor, G. I.: Diffusion by continuous movements, P. Lond. Math. Soc., 20, 196–212, doi:10.1112/plms/s2-20.1.196, 1922.
Weiss, J.: Drift, Deformation, and Fracture of Sea Ice: a Perspective Across Scales, Springer, London, 83 pp., 2013.
Weiss, J. and Marsan, D.: Scale properties of sea ice deformation and fracturing, C. R. Phys., 5, 735–751, 2004.

TCD
8, 4281–4325, 2014

Table 1. Bioy IDs, start and end dates abd location, meander coeficients, triplets.

POB ID	ID	Date (yy/mm/dd) Start	End	Position (Lat, Lon) Start	End	Meander coefficient (09/09/09–09/10/06)	Triplet	Colour
12289100	1	09/09/02	09/10/03	71.092° N, 139.295° W	71.709° N, 153.845° W	1.112	E	Cyan
12287060	2	09/09/08	09/10/06	72.459° N, 136.691° W	72.002° N, 143.999° W	1.259	A	Blue
IMB	3	09/09/09	10/07/11	72.503° N, 136.778° W	77.627° N, 164.588° E	1.318	B	Red
12282070	4	09/09/08	10/02/01	72.513° N, 136.403° W	73.793° N, 174.933° W	1.435	A,B	Blue/Red
12280110	5	09/09/08	09/11/04	72.563° N, 136.699° W	74.373° N, 160.765° W	1.225	A, B	Blue/Red
12286060	6	09/09/08	09/11/30	72.993° N, 135.647° W	73.578° N, 166.991° W	1.238	C	Black
12284060	7	09/09/08	09/12/14	73.069° N, 135.887° W	73.960° N, 165.316° W	1.310	C	Black
12281100	8	09/09/08	09/11/25	73.094° N, 135.552° W	73.917° N, 161.518° W	1.283	C	Black
12283100	9	09/09/04	09/11/04	74.560° N, 136.076° W	73.485° N, 145.958° W	1.755	D	Magenta
12288060	10	09/09/04	09/11/03	74.567° N, 137.324° W	73.552° N, 145.697° W	1.807	D,E	Magenta/Cyan
12288100	11	09/09/04	09/11/16	74.665° N, 137.217° W	73.535° N, 149.796° W	1.671	D,E	Magenta/Cyan

TCD
8, 4281–4325, 2014

Table 2. Buoy triplet longevity.

Triplet	Date (yy/mm/dd) Start	End	Duration (days)
A	09/09/08	09/10/06	28
B	09/09/09	09/11/04	56
C	09/09/08	09/11/25	77
D	09/09/04	09/11/03	59
E	09/09/04	09/10/03	29

TCD
8, 4281–4325, 2014

Table 3. Sea ice divergence/convergence events/intervals, and corresponding approximate locations and dates.

Triplet	Intervals	Location	Date (yy/mm/dd)
A	I (09/10–09/24)	72.5° N, 140° W	09/09/19
B	I	73° N, 137° W	09/09/15
	II (10/09–10/26)	73° N, 145° W	09/10/08
		73° N, 147° W	09/10/15
		73° N, 151° W	09/10/21
C	I	73° N, 137° W	09/16/09
D	I	74.5° N, 136° W	09/14/09
E	I	73° N, 140° W	09/06/09

TCD
8, 4281–4325, 2014

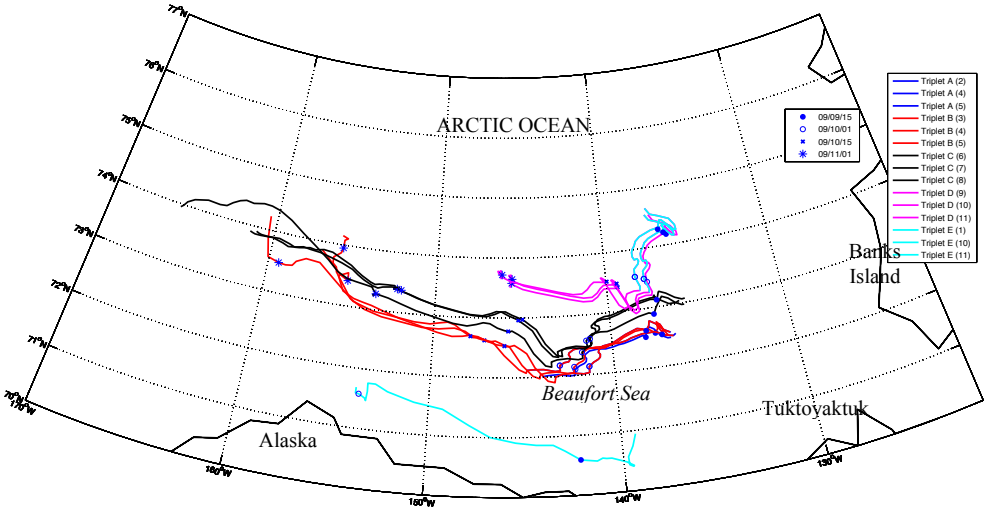

Figure 1a. Map of study area and winter 2009/10 beacon trajectories. Blue, red, black, magenta and cyan indicate triplets A, B, C, D, and E, respectively, with triplet A (E) located nearest to (furthest from) the coastline. Symbols (•, o, x, and *) depict triplet beacon locations on 15 September, 1 and 15 October, and 1 November, respectively, and illustrate enhanced stretching of triplets located closest to the coastline.

TCD
8, 4281–4325, 2014

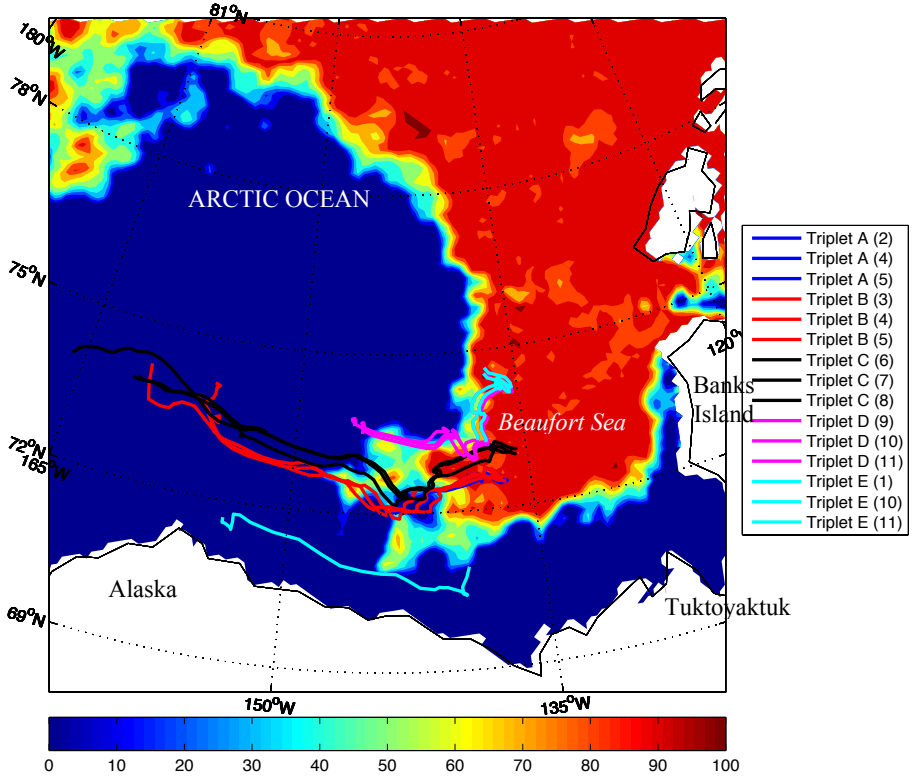

Figure 1b. Map of study area and winter 2009/10 beacon trajectories superimposed on AMSR-E sea ice concentrations for 9 September 2009 and depicting the marginal ice zone on deployment.

TCD
8, 4281–4325, 2014

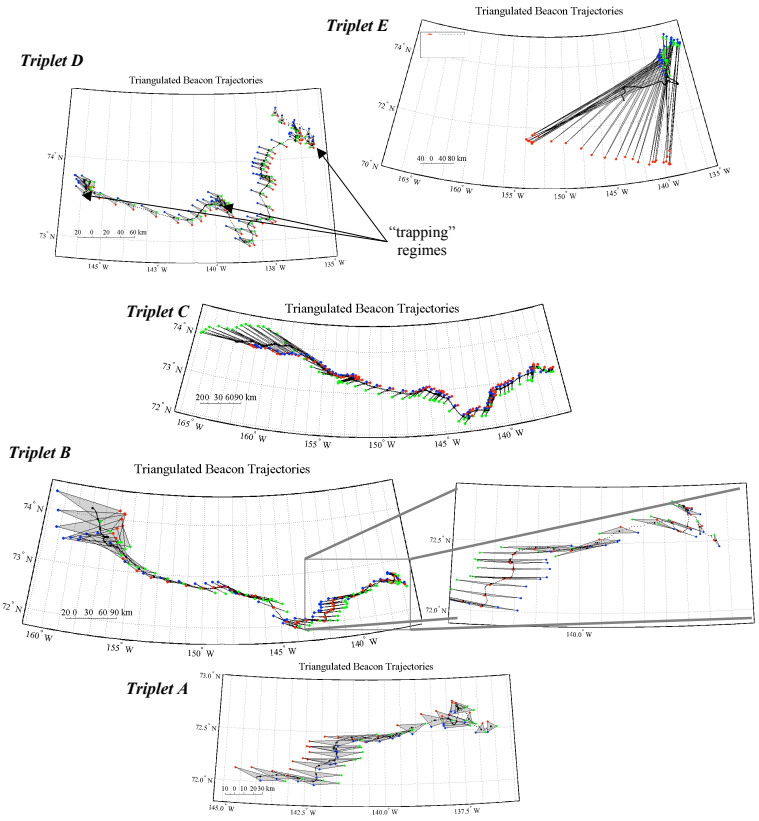

Figure 2. Ice beacon trajectories for (from bottom panel) triplets A, B, C, D, and E. (Note the difference in scale.) Right-hand panel in second row from bottom depicts the initial evolution in triplet B.

TCD
8, 4281–4325, 2014

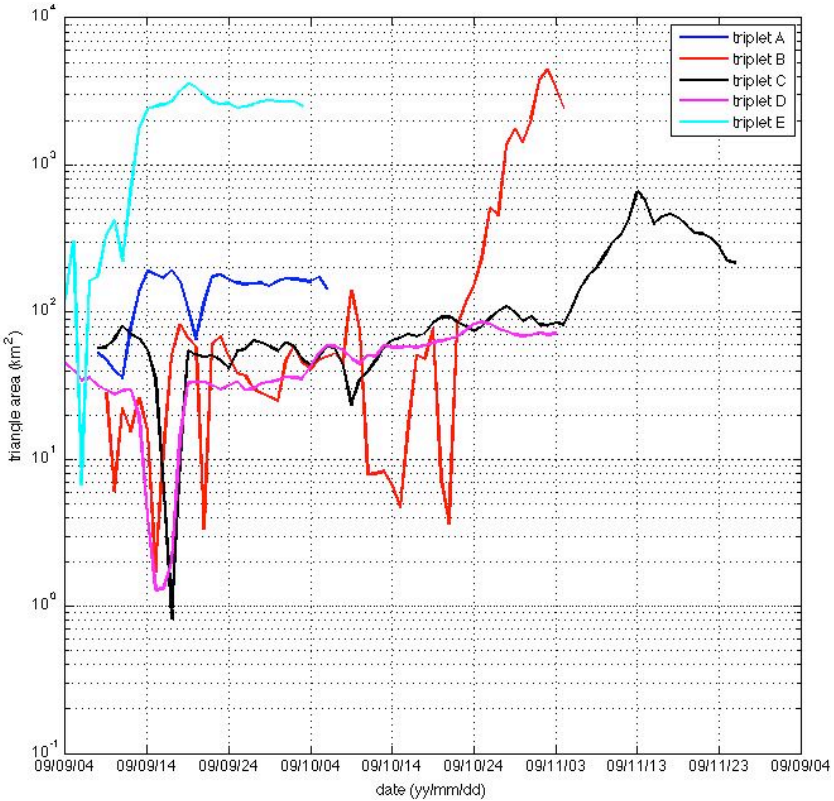

Figure 3. Semilog plot of triangular area by date for ice beacon triplets A to E.

TCD
8, 4281–4325, 2014

Figure 4. Semilog plot of the triangle **(a)** height and base, and the **(b)** aspect (base-to-height) ratio as a function of date for triplets A to E.

TCD
8, 4281–4325, 2014

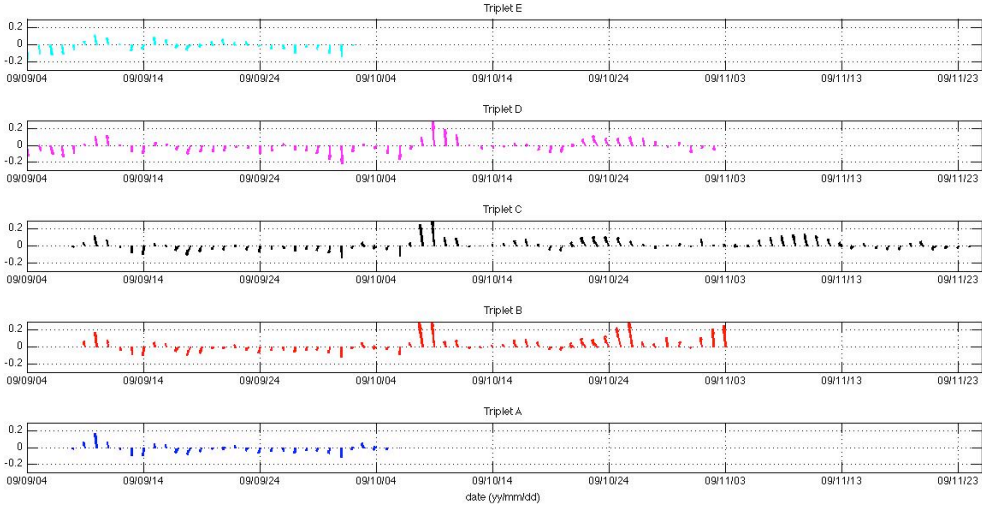

Figure 5. Centroid ice drift velocity (in $m\,s^{-1}$) as a function of date for triplets A (bottom) to E (top).

TCD
8, 4281–4325, 2014

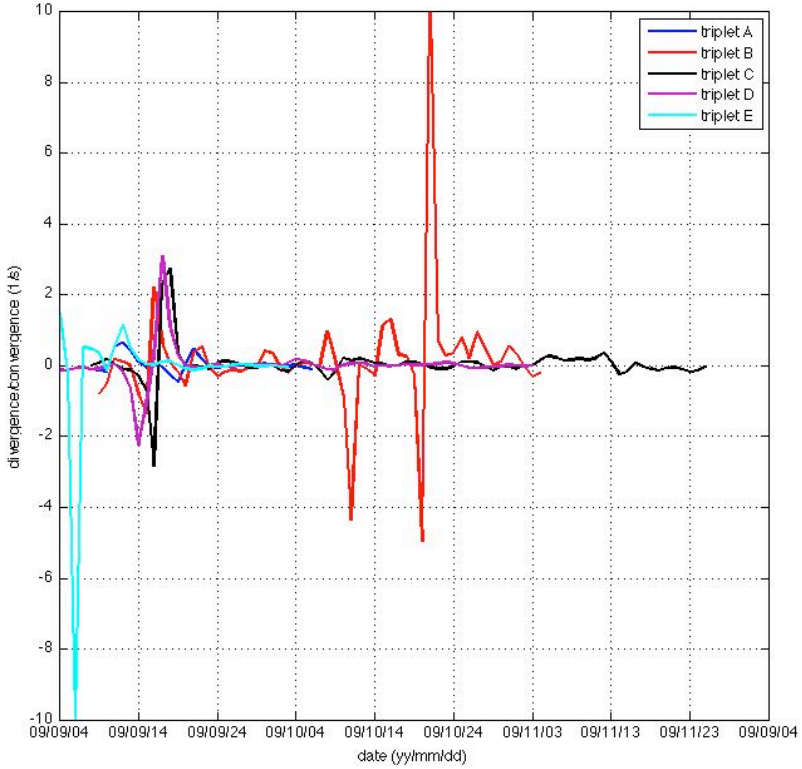

Figure 6. Evolution in sea ice divergence and convergence for triplets A to E.

TCD
8, 4281–4325, 2014

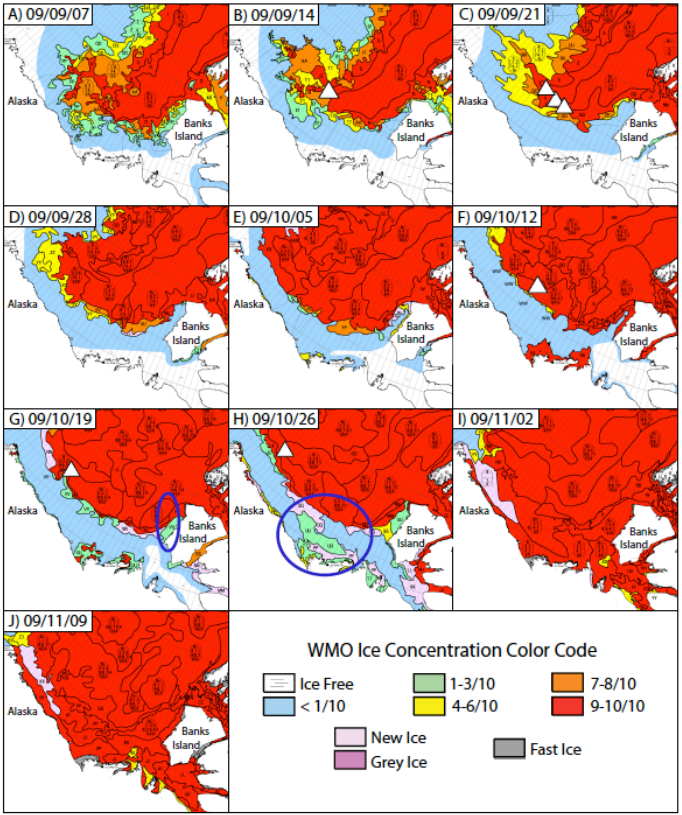

Figure 7a. Canadian Ice Service (CIS) weekly ice charts from 7 September 2009 to 9 November 2009. Ellipses depict the consolidation of marginal ice to the coast and perennial ice pack on 19 and 26 October. Triangles depict the approximate location of triplet centroids during intervals of enhanced divergence/convergence.

TCD
8, 4281–4325, 2014

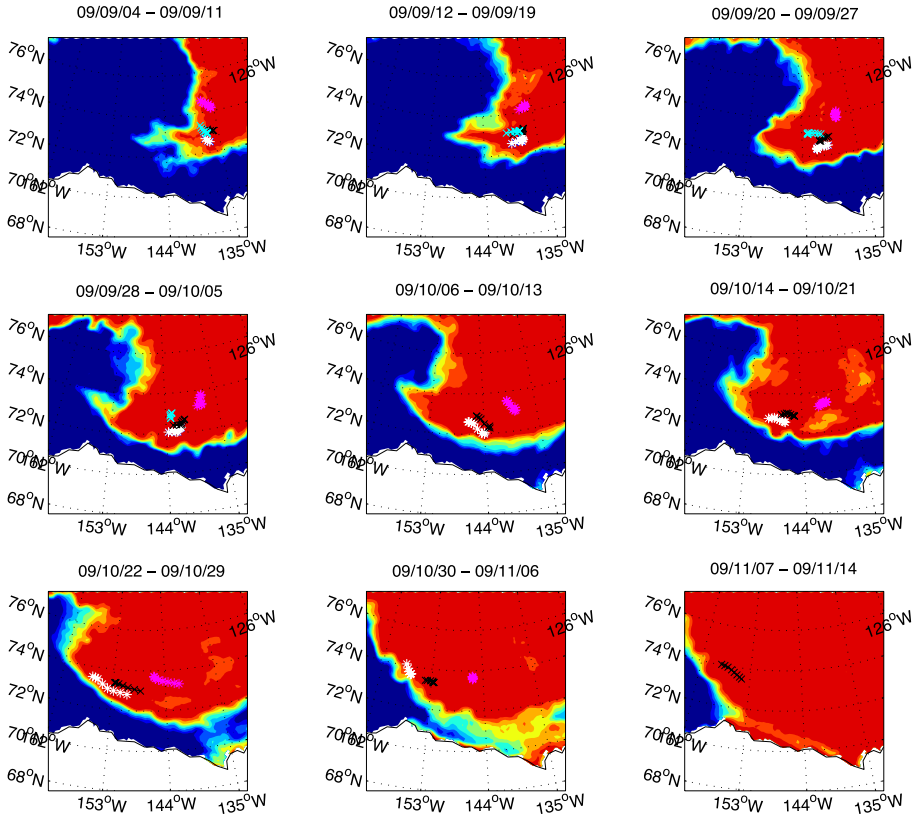

Figure 7b. Maps of weekly AMSR-E sea ice concentrations in addition to weekly evolution in triplet centroids showing proximity of triplets to the ice edge from 4 September 2009 to 14 November 2009.

TCD
8, 4281–4325, 2014

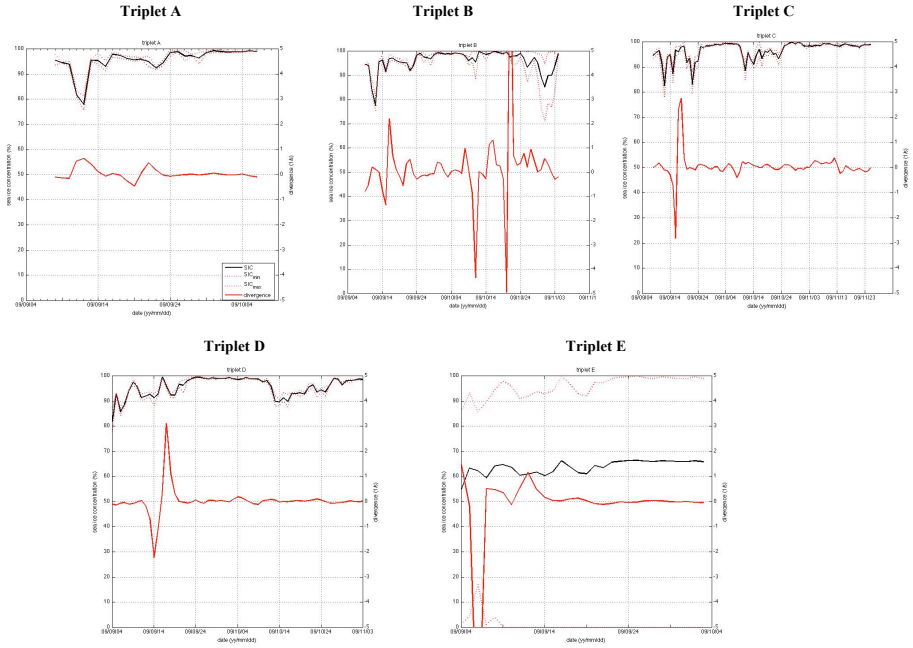

Figure 8. Evolution in mean (black solid line), minimum and maximum (red dashed line, left axis) sea ice concentrations, and divergence (red solid line, right-axis) within a 0.21° triplet centroid radius for triplets A to E.

TCD
8, 4281–4325, 2014

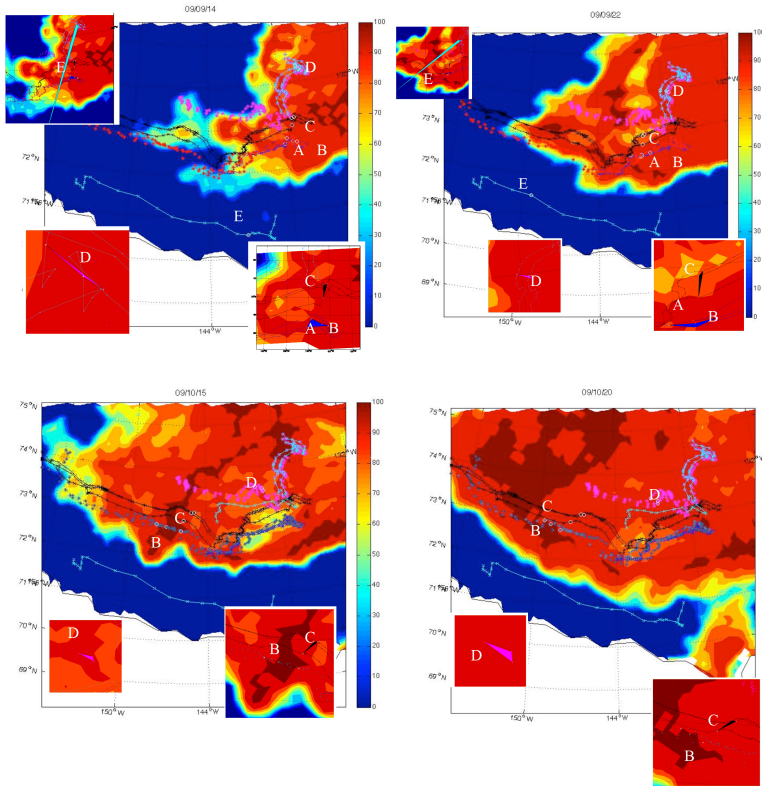

Figure 9. Ice beacon triplet trajectories superimposed on selected daily maps of SIC during intervals of enhanced divergence/convergence (14 and 22 September, and 15 and 20 October, 2009). Note that the trajectory colour for triplet B is red in September and blue-grey in October to distinguish beacon paths from 100 % sea ice concentrations in October.

TCD
8, 4281–4325, 2014

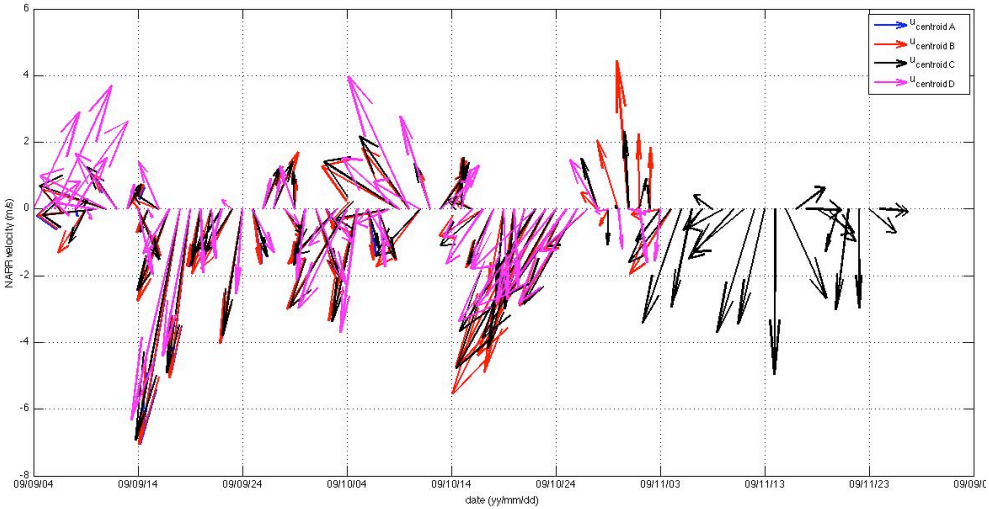

Figure 10. Daily local NARR wind vectors for the area surrounding the triplet centroids from September to November 2009.

TCD
8, 4281–4325, 2014